Article

Cell

Hepatitis C Virus RNA Functionally Sequesters miR-122

Graphical Abstract

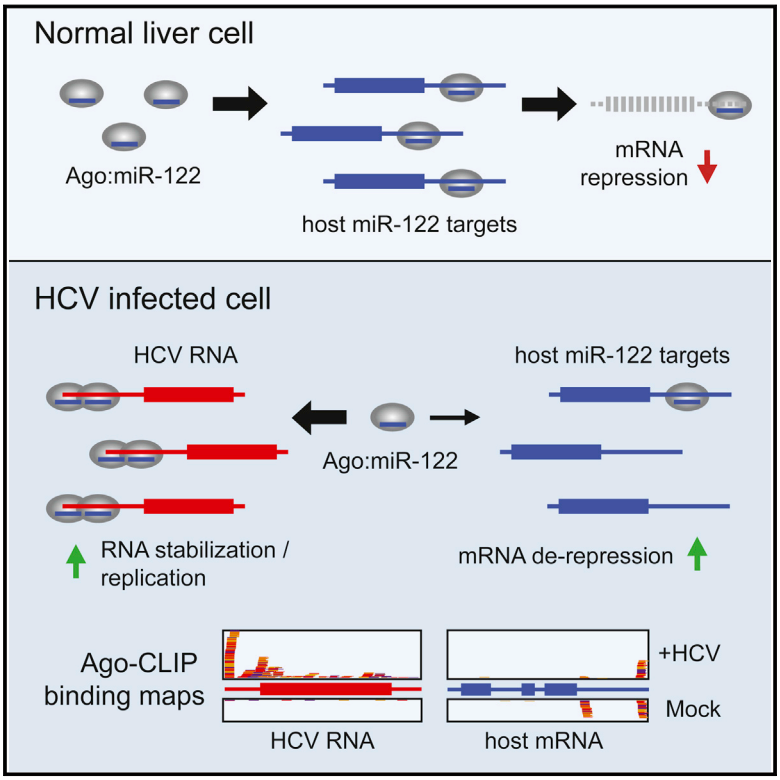

Authors

Joseph M. Luna, Troels K.H. Scheel, ..., Charles M. Rice, Robert B. Darnell

Correspondence

ricec@rockefeller.edu (C.M.R.), darnelr@rockefeller.edu (R.B.D.)

In Brief

Hepatitis C virus uniquely requires the liver-specific tumor suppressor miRNA, miR-122, for its replication. During infection, viral RNA specifically sequesters miR-122 to de-repress its normal host targets, which may facilitate the long-term oncogenic potential of HCV.

Highlights

- Genome-wide miRNA binding profiles were elucidated for HCV infection
- HCV RNA functionally reduces miR-122 binding on endogenous mRNA targets
- HCV miRNA sponging can be redirected by swapping viral miRNA tropism
- Modeling validates single-cell measurements of HCV-induced mRNA de-repression

Accession Numbers

GSE64680

Luna et al., 2015, Cell *160*, 1099–1110
March 12, 2015 ©2015 Elsevier Inc.
http://dx.doi.org/10.1016/j.cell.2015.02.025

CellPress

Article

Cell

Hepatitis C Virus RNA Functionally Sequesters miR-122

Joseph M. Luna,[1,2] Troels K.H. Scheel,[1,3] Tal Danino,[1,4] Katharina S. Shaw,[1] Aldo Mele,[2] John J. Fak,[2] Eiko Nishiuchi,[1] Constantin N. Takacs,[1,5] Maria Teresa Catanese,[1,8] Ype P. de Jong,[1,6] Ira M. Jacobson,[6] Charles M. Rice,[1,*] and Robert B. Darnell[2,7,*]

[1]Laboratory of Virology and Infectious Disease, Center for the Study of Hepatitis C, The Rockefeller University, New York, NY 10065, USA
[2]Laboratory of Molecular Neuro-Oncology and Howard Hughes Medical Institute, The Rockefeller University, New York, NY 10065, USA
[3]Copenhagen Hepatitis C Program (CO-HEP), Department of Infectious Disease and Clinical Research Centre, Copenhagen University Hospital, Hvidovre, and Department of International Health, Immunology and Microbiology, Faculty of Health and Medical Sciences, University of Copenhagen, DK-2200 Copenhagen N, Denmark
[4]Health Sciences and Technology, Massachusetts Institute of Technology, Cambridge, MA 02139, USA
[5]Laboratory of Cellular Biophysics, The Rockefeller University, New York, NY 10065, USA
[6]Center for the Study of Hepatitis C, Division of Gastroenterology and Hepatology, Weill Cornell Medical College, New York, NY 10065, USA
[7]New York Genome Center, 101 Avenue of the Americas, New York, NY 10013, USA
[8]Present address: Department of Infectious Diseases, King's College London School of Medicine, Guy's Hospital, London Bridge, London SE1 9RT, UK
*Correspondence: ricec@rockefeller.edu (C.M.R.), darnelr@rockefeller.edu (R.B.D.)
http://dx.doi.org/10.1016/j.cell.2015.02.025

SUMMARY

Hepatitis C virus (HCV) uniquely requires the liver-specific microRNA-122 for replication, yet global effects on endogenous miRNA targets during infection are unexplored. Here, high-throughput sequencing and crosslinking immunoprecipitation (HITS-CLIP) experiments of human Argonaute (AGO) during HCV infection showed robust AGO binding on the HCV 5′UTR at known and predicted miR-122 sites. On the human transcriptome, we observed reduced AGO binding and functional mRNA de-repression of miR-122 targets during virus infection. This miR-122 "sponge" effect was relieved and redirected to miR-15 targets by swapping the miRNA tropism of the virus. Single-cell expression data from reporters containing miR-122 sites showed significant de-repression during HCV infection depending on expression level and site number. We describe a quantitative mathematical model of HCV-induced miR-122 sequestration and propose that such miR-122 inhibition by HCV RNA may result in global de-repression of host miR-122 targets, providing an environment fertile for the long-term oncogenic potential of HCV.

INTRODUCTION

Hepatitis C virus (HCV) is a hepatotropic positive-strand RNA virus of the Flaviviridae family that is a leading cause of liver disease globally, with morbidities such as fibrosis, cirrhosis, and hepatocellular carcinoma (Yamane et al., 2013). The long ORF of the ~9.6 kb HCV genome encodes a polyprotein processed into ten proteins and is flanked by critical structured UTRs. Unique to this virus is a dependence on the liver-specific microRNA-122 (miR-122) (Jopling et al., 2005). Whereas miRNAs typically interact with the 3′UTRs of mRNAs to promote mRNA destabilization and/or translational repression (Bartel, 2009), the binding of miR-122 to two binding sites (seed site S1 and S2) in the 5′UTR of HCV genomic RNA is critical for viral replication (Jopling et al., 2008; Machlin et al., 2011) by moderately stimulating viral protein translation (Henke et al., 2008) and, in concert with Argonaute (AGO), by stabilizing and protecting the uncapped HCV RNA genome from degradation (Li et al., 2013b; Sedano and Sarnow, 2014; Shimakami et al., 2012). As the predominant miRNA in the liver, miR-122 has multiple roles to regulate lipid metabolism (Esau et al., 2006), iron homeostasis (Castoldi et al., 2011), and circadian rhythms (Gatfield et al., 2009). MiR-122 knockout studies in vivo have revealed potent anti-inflammatory and anti-tumorigenic functions (Hsu et al., 2012; Tsai et al., 2012). Antagonizing miR-122 as an HCV therapeutic is a novel strategy (Lanford et al., 2010) with the first-in-class inhibitor, miravirsen/SPC3649, currently in phase II clinical studies (Janssen et al., 2013).

Studies of miRNA action during virus infections have been enhanced with the advent of high-throughput methods to elucidate genome-wide miRNA:mRNA interaction networks biochemically. Such methods (Chi et al., 2009; Hafner et al., 2010), broadly relying on cross-linking and immunoprecipitation (CLIP) of RNA bound to protein, have been applied to latent Kaposi's sarcoma-associated herpesvirus (KSHV) (Haecker et al., 2012) and Epstein Barr virus (EBV) infections to uncover miRNA regulatory networks involved in promoting viral latency (Skalsky et al., 2012) and regulating cellular apoptosis (Riley et al., 2012).

In the current study, we elucidated global miRNA:target interaction maps during HCV infection on host and viral RNA. We observed AGO engagement at the HCV 5′UTR miR-122 sites, describe replication-dependent argonaute binding throughout

viral genomic RNA, and provide evidence of miR-122 binding on an HCV resistant to miR-122 antagonism. On the host transcriptome, our results revealed globally reduced AGO binding and specific de-repression of miR-122 targets upon virus infection. This surprising systems-level observation suggests that HCV RNA functionally sequesters miR-122, and exhibits a miRNA "sponge" effect analogous to roles proposed for competing endogenous RNAs (ceRNA) (Salmena et al., 2011). Taken together, our results establish an RNA virus as a specific and indirect regulator of miRNA activity in the cell.

RESULTS

Argonaute HiTS-CLIP of HCV Infected Cells

To study miRNA interactions during HCV infection, we either electroporated RNA or infected Huh-7.5 hepatoma cells with J6/JFH1-Clone2 HCV and after 48–72 hr, when most cells were infected, performed AGO-CLIP and RNA-seq measurements (Figures S1A–S1C). AGO-CLIP was performed using linker ligation as previously described (Figures S1D–S1F) (Moore et al., 2014). Alignment statistics for CLIP datasets presented in this paper are summarized in Tables S2, S3, S4, and S5.

Due to known linker ligation biases in the preparation of small RNA libraries (Zhuang et al., 2012), we used polyG tailing (adapted from Ingolia et al., 2009) to determine miRNA abundance profiles (Figure S1G), and found that miR-122 at ~4.9% is the seventh most abundant miRNA (Figure S1H and Table S1). This correlated with previous data on miR-122 abundance in these cells (Figures S1I and S1J). No systematic bias from linker ligation was observed on mRNA targets due to the relative heterogeneity of RNaseA cleavage in creating mRNA AGO footprints (Figures S1K and S1L). For subsequent analysis on mRNA-CLIP clusters, we focused on searching the top 50 seed families derived from poly-G CLIP studies, which constituted over 97% of miRNAs identified in Huh-7.5 cells.

An AGO Binding Map of HCV RNA Confirms Extensive miR-122 Engagement

To define a small RNA interaction map on HCV and human mRNA, CLIP reads were mapped onto the HCV and human genomes. Among the 1%–2% of CLIP reads mapping to HCV, AGO binding sites were identified by clustering overlapping reads and identifying statistically significant peaks above a uniformly distributed background (Darnell et al., 2011; Licatalosi et al., 2012). We observed major peaks in the 5′UTR, E1, E2, NS5A, and NS5B regions of the genome (Figure 1A, top). No significant binding was observed on the negative strand (data not shown). Notably, 50% of all AGO binding events on HCV RNA overlapped the known miR-122 seed sites in the 5′UTR (Figures 1A and 1B). Achieving nucleotide precision on the AGO:mRNA crosslink site via crosslink-induced mutation site analysis (CIMS [Zhang and Darnell, 2011]), we observed an enrichment of crosslink sites predominantly within and immediately upstream of S2 (at positions 28 and 35) and, to a lesser degree, S1 base pairing locations (Figure 1B). The second largest peak was observed in the HCV IRES and overlapped the pseudoknot and coding start site (Figure 1D). No canonical 7-mer or 8-mer binding sites for the top 50 miRNA seeds were noted in this region; however, a putative non-canonical miR-122 site in the IRES (Pang et al., 2012) may explain the observed AGO binding.

To probe the general miRNA dependence of AGO binding on HCV RNA and to specifically enrich for miR-122-dependent binding, we deleted Drosha from Huh-7.5 cells to globally disrupt most miRNA biogenesis, using a CRISPR-based genome editing strategy (Figure S2). From CLIP in ΔDrosha supplemented with miR-122 mimic to support HCV infection (Figure S2G), we observed that binding to S1/S2 and the IRES was maintained, and notably enhanced at NS5B binding sites (Figures 1A and 1C), both of which contain conserved miR-122 sites (Figure S3), of which one was previously shown to be inhibitory for HCV replication (Nasheri et al., 2011). AGO binding to E1 and E2 peaks was reduced in ΔDrosha cells, suggesting that a minor proportion of AGO binding on HCV RNA is due to other miRNAs. While reports have suggested that numerous miRNAs interact with HCV RNA (reviewed in Singaravelu et al., 2014), among these only let-7 and miR-196 families fell within the top 50 miRNAs expressed, and no seeds from either of these families were observed within significant AGO binding peaks. Taken together, these data suggest that miR-122 constitutes the predominant miRNA interaction with HCV RNA in these cells and is largely confined to the 5′UTR.

AGO Binding to miR-122 Sites on HCV RNA Occurs Early and Is Replication Independent

To address the timing of AGO binding to HCV RNA, we performed CLIP over a time course after electroporation of WT or replication defective (GNN) RNA genomes. We observed comparable AGO binding at the S1/S2 sites of WT and GNN mutants as early as 6 hr post-electroporation (Figures 1E and 1F). AGO binding to the 5′UTR in general, and to miR-122 sites in particular, remained stable throughout the WT time course but decreased steadily for the GNN mutant. AGO binding to regions outside the 5′UTR emerged after 24 hr, were not observed in the GNN mutant, and correlated with HCV RNA abundance over time (Figures 1E–1G). This suggested early AGO binding to the 5′UTR and additional replication or abundance-dependent low-level AGO targeting of the viral ORF.

An HCV Resistant to miR-122 Antagonism Engages miR-122 and AGO

To further dissect the impact of non-miR-122 AGO binding on HCV RNA, we focused on an HCV recombinant that is resistant to miR-122 antagonism (Li et al., 2011). This virus, for which the first HCV 5′UTR stem-loop is replaced with cellular U3 snoRNA, lacks the S1 site but contains an intact S2 site. Upon deleting miR-122 from Huh-7.5 cells (ΔmiR-122) using a CRISPR-based strategy (Figure S2), we observed that while WT virus replication was abolished in ΔmiR-122 cells, U3 virus replication was largely unaffected (Figures 2A and 2B). Reintroducing miR-122 completely rescued WT virus replication and had a small but consistent (2- to 4-fold) proviral effect on the U3 virus (Figures 2A and 2B), suggesting that U3 virus replication is largely miR-122 independent. U3 virus replication could also be launched in ΔDrosha cells, yet in WT cells S2 p3 and p3,4 mutants were negative for HCV replication over 3 weeks, suggesting perturbation of overlapping functions on the RNA (data not shown). In CLIP on U3

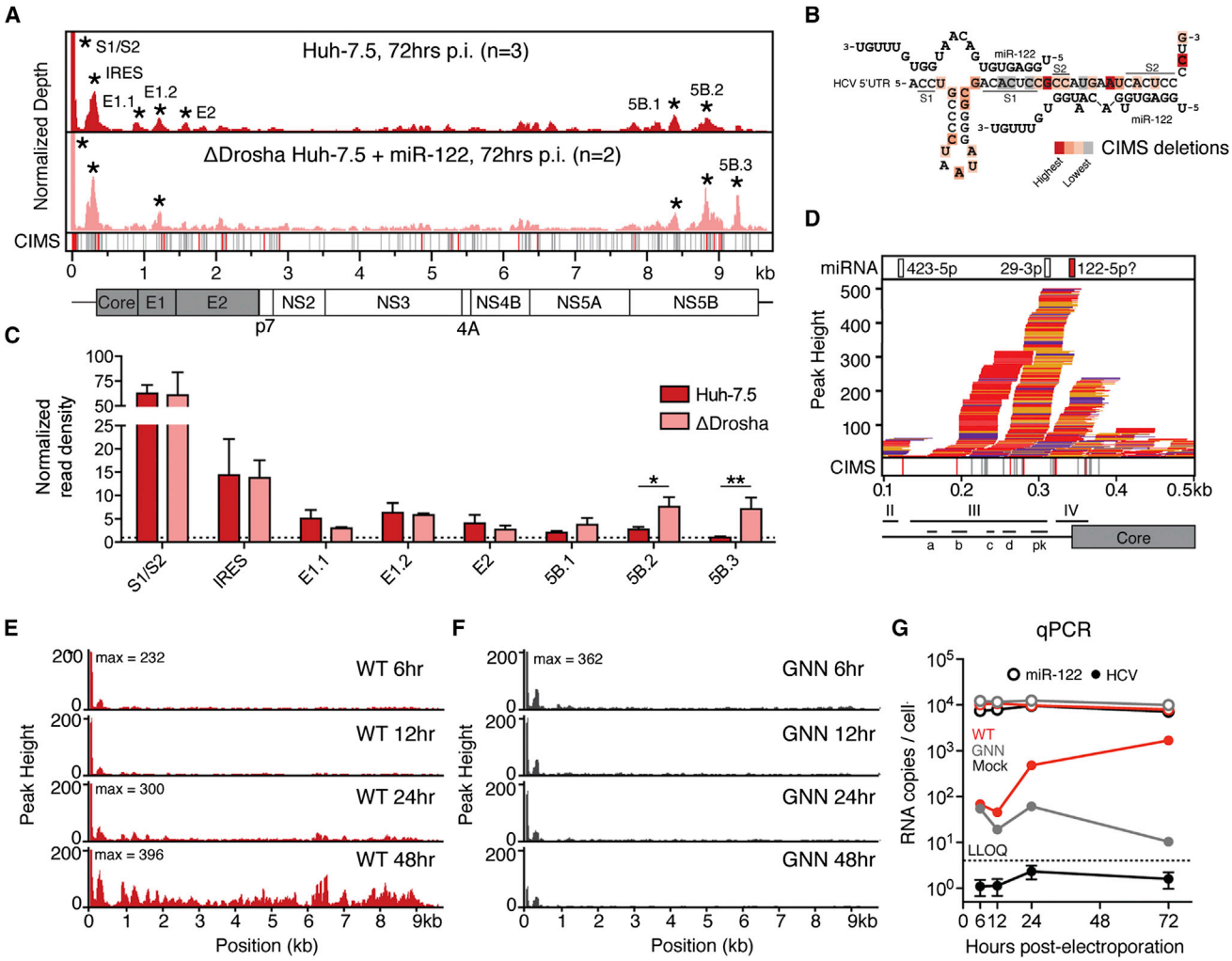

Figure 1. Argonaute Binding Maps on HCV RNA

(A) Mock-subtracted binding map of AGO-CLIP reads across HCV genomic RNA in WT or ΔDrosha Huh-7.5 cells. Data were normalized to total cellular and virus read depth for comparison. Significant peaks per track are named by location and indicated by asterisks. Bottom CIMS track shows location of all deletions (gray) and statistically significant CIMS deletions (red) from the WT track.

(B) AGO binding in significant peaks from WT Huh-7.5 cells in (A) shown as normalized read densities calculated per dataset. Data were normalized to background read density of non-peak regions (dashed line). Asterisks, $^{**}p < 0.01$, $^{*}p < 0.05$, Student's t test. Error bars, ± SD.

(C) Schematic of a miR-122 binding model to S1 and S2 highlighting locations of CIMS deletions.

(D) Zoom in view of AGO binding from WT cells in (A) across the viral IRES into the coding sequence. IRES domains (II-IV), associated stemloops (a-d), and the pseudoknot (pk) region are indicated. Upper track displays seeds for the top 50 miRNA seeds, previously proposed miR-122 binding (Pang et al., 2012) highlighted in red.

(E and F) AGO binding time course of WT (E) and replication deficient (GNN) (F) HCV post-electroporation (n = 2).

(G) Absolute qPCR measurements of miR-122 and HCV RNA levels at indicated time points post-electroporation (n = 3). Replication-deficient J6/JFH1-GNN and mock controls are shown. Dashed line indicates lower limit of quantitation. Error bars, ± SD. See also Figure S3.

infected Huh-7.5 cells, we observed AGO binding and crosslink mapping at the S2 miR-122 site specifically (Figure 2C) mirroring WT virus and indicating that the U3 viral RNA residually engages miR-122. In the presence of increasing concentrations of miR-122 locked nucleic acid (LNA) inhibitor, we observed a dose-dependent decrease in AGO binding across the viral ORF, and a significant decrease in the S2 and IRES binding locations (Figures 2D and 2E), consistent with a limited proviral effect of miR-122 and specific miR-122 binding to S2 and the IRES. Furthermore, S2 and IRES binding was lost in U3 infected ΔDrosha and ΔmiR-122 cells (data not shown). The striking miR-122 independence of this virus points to a potential avenue of resistance to LNA-based therapeutics in the form of recombinant viruses with similarly large 5′UTR stem-loops.

HCV Infection Functionally Reduces Argonaute Binding on Host miR-122 Targets

Given the crucial requirement of miR-122 for HCV replication, and in light of the result that HCV RNA levels accumulate to within one log of miR-122 levels (Figure 1G), we hypothesized that the HCV

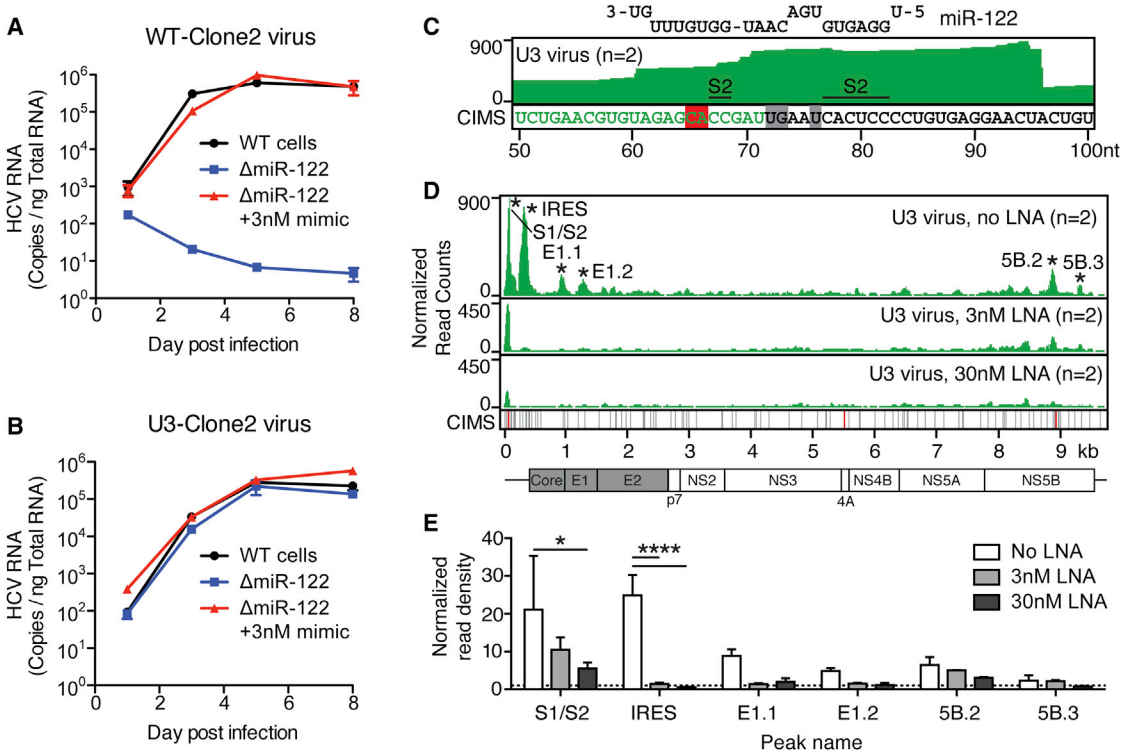

Figure 2. An HCV Mutant Resistant to miR-122 Antagonism Engages AGO and miR-122

(A and B) Time course qPCR measurements of WT-Clone2 virus (A) or U3-Clone2 virus (B) in WT cells or in ΔmiR-122 cells with or without 3 nM miR-122 supplementation. Error bars, ± SD.

(C) AGO binding map (top track) and CIMS locations (bottom track) across the U3 virus 5′UTR corresponding to miR-122 binding at S2. Relevant CIMS deletions are shown in gray (not significant) and red (significant). U3 snoRNA sequence is shown in green.

(D) AGO binding map across the U3 virus genome after treatment with increasing doses of LNA122. Significant peaks are named by location and indicated by asterisks. Bottom CIMS track shows location of all deletions (gray) and significant CIMS deletions (red) for the untreated dataset.

(E) AGO binding in significant peaks from untreated U3 datasets in (D) shown as normalized read densities calculated per dataset. ****$p < 0.0001$, *$p < 0.05$, one-way ANOVA with bonferroni correction. Error bars, ± SD.

genome may act as a "sponge" for cellular miR-122, where viral replication may exert a broadly de-repressive effect on host miR-122 targets. We reasoned that this effect would be noticeable via CLIP as reduced AGO binding of miR-122 targets upon infection that may result in a specific increase in the expression of these targets measured by mRNA-seq. Indeed, comparing HCV infected to uninfected cells, we observed significantly reduced AGO binding globally for mRNA targets for which a miR-122 seed was present, compared to the combined targets of the miR-15/16 family, as a representative targetome of similar size to the miR-122 target network, and the top 10 or the top 50 miRNA families cumulatively (Figure 3A). Significant changes in miR-122 binding were observed for all canonical seed types (as defined in Bartel, 2009) (Figure 3B). Additionally, the greatest change in AGO association was observed in CLIP clusters within 3′UTRs and was less significant in CDS (coding exons), 5′UTRs, and introns (Figure S4A). Notably, the 3′UTR targets of other miRNAs suggested to bind HCV RNA directly were not altered upon HCV infection (Figure S4B). Through RNA-seq measurements we observed functional de-repression of CLIP-derived miR-122 3′UTR targets after virus infection such that greater RNA abundance was evident when compared to all miRNA targets (Figure 3C). Likewise, we observed significant expression changes for all miR-122 target seed types (Figure 3D). Compared to bioinformatic prediction using Targetscan6.2 (TS) (Lewis et al., 2005), we found that CLIP largely complemented and expanded upon predicted miR-122 targets (Figures S4C–S4G). 3′UTR targets identified via CLIP and predicted by TS exhibited the greatest change in AGO binding (Figure S4C) and mRNA de-repression (Figures S4D and S4E) compared to expressed targets unique to either search modality. Of the expressed 731 miR-122 CLIP targets of all seed types identified via CLIP, 48% and 9% overlapped with non-conserved and conserved TS predictions, respectively (Figure S4F). Focusing on a more stringent set of 7-mer and 8-mer seeds for CLIP data yielded even greater overlap, such that only 5% of CLIP-derived targets were not represented in either TS conservation category (Figure S4G). These results highlight a broad convergence between CLIP and bioinformatic prediction to outline a set of miR-122 targets specifically derepressed upon virus infection.

To further corroborate our CLIP observations with HCV infection, we performed CLIP after pharmacologic inhibition of miR-122 and in ΔmiR-122 Huh-7.5 cells. The reduced AGO binding on miR-122 3′UTR targets during HCV infection was similar to

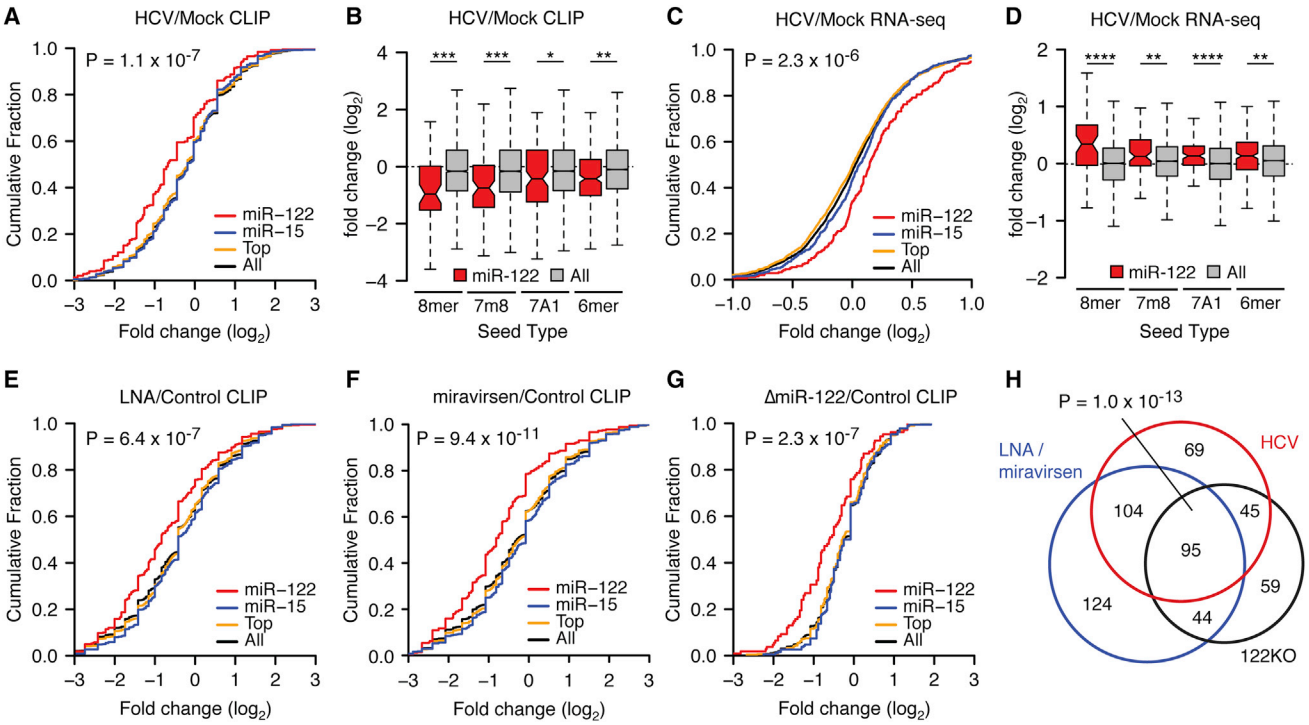

Figure 3. HCV Infection De-Represses Endogenous miR-122 Targets

(A) Cumulative density function (CDF) of the $\log_2$ fold change in CLIP binding between infected and uninfected cells for all 3′UTR clusters containing indicated 7- to 8-mer seeds by family, from triplicate experiments. "Top" refers to the top 10 miRNA families, exclusive of miR-122. "All" refers to the top 50 miRNA families, inclusive of miR-122. Two-sided K-S test p value between miR-122 and all targets shown.

(B) The mean $\log_2$ fold change (±ranges) in CLIP binding on miR-122 3′UTR targets versus all targets during HCV infection broken down by seed type.

(C) A CDF plot during HCV infection as in (A) but measuring target mRNA expression via RNA-Seq, from duplicate experiments at 72 hr post-infection. Targets with more than one miRNA binding site were collapsed such that no gene is represented more than once per category.

(D) The mean $\log_2$ fold change (± ranges) in mRNA expression of CLIP targets during HCV infection broken down by seed type.

(E–G) CDF plot as in (A), between treatment over control cells with LNA122 (E) or miravirsen (F) at 30 nM or genetic deletion (G) of miR-122 (ΔmiR-122), each from triplicate experiments.

(H) Proportional Venn diagram showing the overlap of miR-122 targets with reduced CLIP binding across ΔmiR-122, LNA or miravirsen treatment, and HCV infection conditions. Hypergeometic p value of overlap shown.

Asterisks: ****p < 0.0001, ***p < 0.001, **p < 0.01, *p < 0.05, two-sided Mann-Whitney U-test. See also Figures S2 and S4.

30 nM LNA122 or miravirsen treatment (Figures 3E and 3F) and to ΔmiR-122 cells compared to unedited controls (Figure 3G). Interrogating the list of 3′UTR targets exhibiting reduced AGO binding across these three conditions revealed highly significant overlap (Figure 3H), suggesting that the effect of HCV replication on lowering functional miR-122 levels is functionally similar to antagonizing miR-122. The full complement of miRNA targets identified in these studies is presented in Table S6.

Transcriptome Regulation by miR-122 Sequestration In Vitro Is Predictive of Sequestration In Vivo

As the global effect of HCV replication on host miR-122 usage mirrored LNA inhibition, and more profoundly miR-122 deletion, we hypothesized that miR-122 targets as a class might be de-repressed in human livers as a result of HCV infection. To this end, we performed a meta-analysis of published liver biopsy microarray data related to miR-122 inhibition or HCV infection. Comparing TS predictions for expressed miR-122 or miR-15 targets, as well as CLIP-identified miR-122 targets to all expressed genes in microarray data from miravirsen-treated chimpanzee livers (Lanford et al., 2010), we noted a significant de-repression for TS or CLIP miR-122 targets compared to all genes or to predicted miR-15 targets (Figure 4A). In this dataset, the CLIP-identified miR-122 targetome as a group was broadly more de-repressed than TS predictions. We performed the same analysis comparing HCV infected versus uninfected samples from two array datasets (Mas et al., 2009; Peng et al., 2009) and, despite the unknown proportion of infected cells, found in both that miR-122 target predictions were significantly de-repressed compared to all genes or to miR-15 target predictions in both datasets (Figures 4B and 4C). While these results cannot directly confirm an HCV sponge effect in vivo, they do emphasize that the overlap between CLIP results in vitro and expression results in vivo may indicate specific de-repression of miR-122 targets during HCV infection.

Validation of HCV-Induced miR-122 Sequestration in Bulk and Single Cells

The results thus far describe the global characteristics of the HCV-induced miR-122 sponge effect on the host transcriptome.

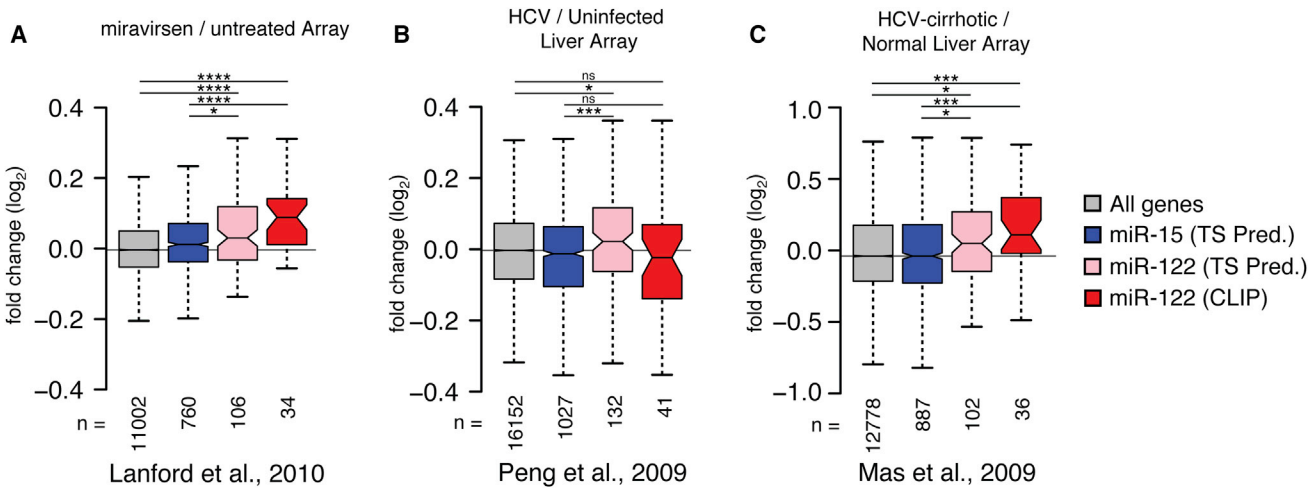

Figure 4. Meta-Analysis of Published Array Data Suggests HCV-Induced Changes on the miR-122 Target Network

(A) Miravirsen pre- and post-treatment array data from four HCV infected chimpanzees (Lanford et al., 2010) was binned according to conserved 7- to 8-mer TargetScan (TS) predictions for miR-15 or miR-122, or from miR-122 targets with CLIP support from the current study. Boxplot whiskers denote 1.5 times the inter-quartile distance from the nearest quartile. The mean fold change in expression for miR-122 targets was compared to miR-15 targets or all genes represented on the array, where the number of genes in each bin (n) is indicated.

(B) Analysis as in (A) comparing 24 HCV-positive to 5 -negative liver biopsies (Peng et al., 2009).

(C) Analysis as in (A) comparing 41 HCV-positive with cirrhosis samples to 19 normal livers (Mas et al., 2009).

Asterisks: ****$p < 0.0001$, ***$p < 0.001$, **$p < 0.01$, *$p < 0.05$, ns $p > 0.05$, two-sided Mann-Whitney U-test.

We next used luciferase and fluorescent reporters of miRNA activity to validate the HCV miR-122 sponge on individual 3′UTRs. The endogenous repression of luciferase reporters containing one miR-122 seed, as well as 3′UTRs of CLIP-derived miR-122 targets was enhanced upon adding additional miR-122 and was reversed upon LNA-mediated miR-122 inhibition (Figure 5A). We also observed seed-dependent statistically significant de-repression of these reporters upon virus infection (Figure 5A).

As cellular mRNA and HCV RNA expression levels can vary widely between individual cells (Kandathil et al., 2013; Sheahan et al., 2014), we sought to achieve a more thorough understanding of the HCV miRNA sponge on host miRNA targets at a quantitative single-cell level. Previous work demonstrated that miRNAs generate thresholds of gene expression such that miRNA repression can be highest on low abundance targets and can be virtually non-existent on high-abundance targets. Furthermore, these thresholds can be altered upon manipulating miRNA levels (Mukherji et al., 2011). To test whether HCV replication could broadly impact functional miR-122 levels, we adapted the strategy used by Mukherji et al. to construct two-color tet-inducible fluorescent reporters of miRNA activity amenable to flow cytometry (Mukherji et al., 2011) (Figure 5B).

Testing reporters with N = 1 and 6 miR-122 binding sites in the presence of miR-122 mimic, we observed miR-122 repression that increased with *N*, as expected, whereas adding LNA122 decreased repression (Figure S5A–S5D). HCV infection in both contexts resembled LNA inhibition where de-repression was notably more pronounced in cells expressing low amounts of reporter, demonstrating previously reported miRNA thresholding effects (Mukherji et al., 2011) (Figures S5A and S5C). Importantly, no such changes were observed for a reporter with a p3,4 miR-122 seed ("N1m"). (Figures S5E and S5F). Additionally, we tested a reporter with a perfectly complementary miR-122 site, thus making the miRNA behave as an siRNA. This reporter exhibited no thresholding such that mimic repression, or LNA and HCV de-repression was observed at all expression levels (Figures S5G and S5H). These data suggest that HCV infection modulates functional miR-122 levels to relieve endogenous repression on host targets in a stoichiometric manner, governed by target expression level and the number of miRNA binding sites.

As miR-122 levels in Huh7-derived cells are estimated to be 10-fold lower than primary adult liver tissue (Chang et al., 2004), we next explored the HCV sponge effect in the presence of excess miR-122. Exogenous miR-122 addition increaseed intracellular miR-122 by up to 10-fold in Huh-7.5 cells, within the range of miR-122 levels measured from patient liver biopsies (Figures S6A and S6B). As no changes in HCV RNA levels were observed, the resulting miR-122:HCV ratio went from ~15:1-fold at the lowest, to over 100:1 with 30 nM of miR-122 mimic added (Figure S6C). Testing N = 1 or AldoA 3′UTR reporter constructs in this in vivo-like context, we observed that HCV infection was able to relieve 30 nM of mimic repression to untreated levels for low but not high abundance targets (Figures 5C and 5D). The ability for HCV to rescue excess miR-122 repression was not as pronounced for the N = 4 construct (Figure 5E) whereas a reporter containing a perfectly complementary miR-122 site was particularly sensitive to rescue by HCV replication (Figure 5F). Similar, dose-dependent results were obtained under 0.3 or 3 nM mimic treatment for all constructs (Figures S6D–S6G). Taken together, these results suggest that miR-122 sponging by HCV can exist in more physiologic miR-122 concentration settings.

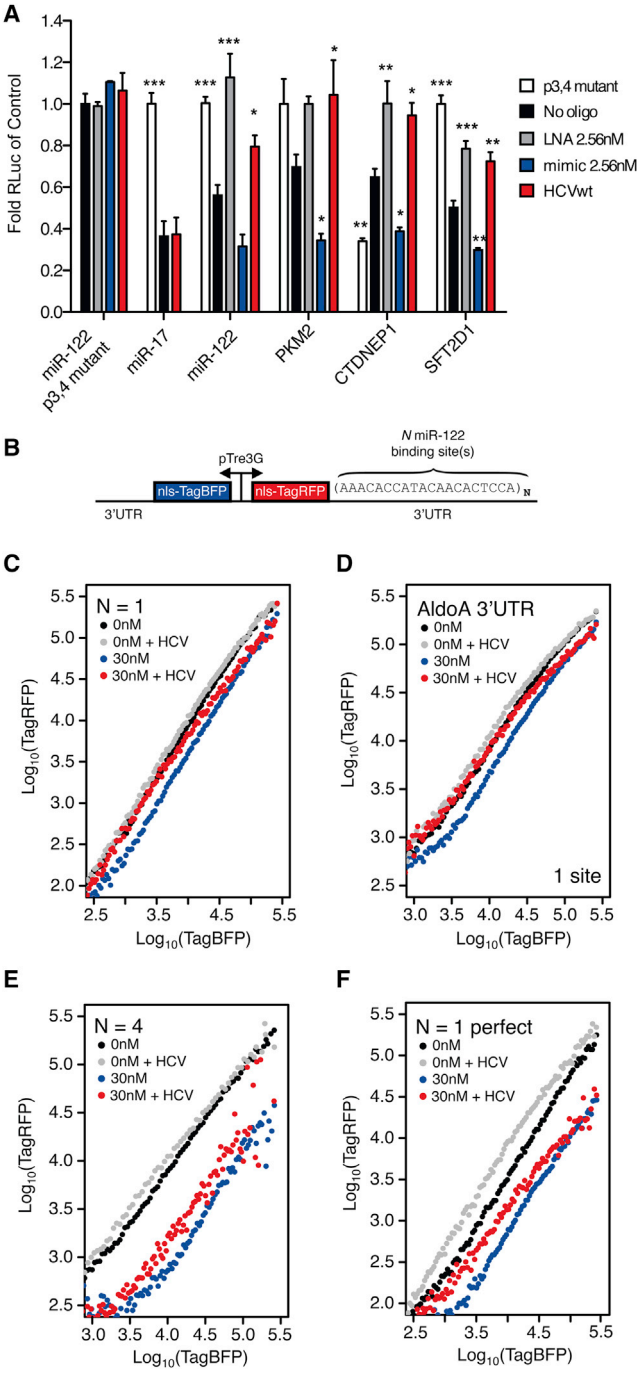

Figure 5. Validation of HCV-Induced De-Repression of miR-122 Targets in Bulk and Single-Cell Resolution

(A) Luciferase reporter measurements for synthetic miR-122, miR-17, or cellular 3′UTR target constructs. Data were normalized to "no oligo" p3,4 mutant conditions. Significance testing was performed relative to endogenous "no oligo" repression for each tested construct. Error bars, ± SEM. Asterisks: ***p < 0.001, **p < 0.01, *p < 0.05, ANOVA with Bonferroni correction.

(B) Two-color fluorescent reporter containing a bidirectional Tet promoter that drives expression of blue and red fluorescent proteins (TagBFP and TagRFP). Each fluorescent protein is tagged with a nuclear localization sequence (NLS) to aid in flow cytometric analysis. The 3′UTR of TagRFP is engineered to contain *N* binding sites for miR-122, or full 3′UTRs of miR-122 targets.

(C–F) Log-log transfer functions for N = 1 (C), ALDOA 3′UTR (D), N = 4 (E) or one perfectly complementary (F) miR-122 site in the presence or absence of 30 nM miRNA mimic and/or HCV infection.

A Quantitative Model of miR-122 Sponging by HCV RNA

To achieve a more quantitative understanding of the HCV sponge, we used our dose-dependent mimic and LNA reporter system measurements to expand the miRNA model of gene regulation presented by Mukherji et al. to incorporate a competing self-replicating viral target (Figure 6A). Here, if HCV RNA is present at sufficiently high numbers or has relatively high-binding strengths compared to other miR-122 targets, it acts to reduce the available miR-122 pool, and de-represses miR-122 targets (r, measured as TagRFP fluorescence) relative to non-targets (r_0, measured as TagBFP fluorescence) (Figure 6B). We developed a quantitative formula for HCV-induced reduction of the miR-122 pool in this scenario (see Supplemental Information). Assuming steady-state levels of HCV RNA at the time of measurements resulted in a decrease of the model parameter θ, which governs the amount of free miRNA in the system. The number of miR-122 sites is estimated by the model parameter λ that is related to the total binding strength of miR-122 to a particular site. By tuning these parameters, we accurately fitted experimental data of endogenous miR-122 repression of reporters with increasing numbers of miR-122 sites (Figure 6C).

To explore the effect of HCV on the miR-122 pool, we fitted the model to experimental data with four miR-122 sites during infection (Figure 6D), and estimated the change to parameter θ to correspond to an approximate 50% reduction in available miR-122. A similar result was obtained for the N = 4 construct in the presence of HCV and 30 nM miR-122 mimic (Figure 6E). The model estimated that the highest theoretical HCV levels reducing the miR-122 pool by 90% could de-repress mRNA targets by up to 4.5-fold for low-expressed mRNAs (Figure 6F). Synthetic reporter measurements agreed with model predictions for 50% reductions in miR-122 levels, where de-repression was most drastic for low expressed targets harboring multiple miR-122 sites (Figure 6G).

In similar measurements with reporters containing full 3′UTRs, we observed modest de-repression upon HCV infection with an average change of 25% across all expression levels for the previously known targets with one miR-122 site, AldoA, PKM2, and P4HA1, but not for CS 3′UTRs (Figures 6H and S5H–S5L). The novel CLIP-identified targets CTDNEP1, SFT2D1, MASP1 and MAL2 behaved similarly, with all four tested being reduced upon miR-122 mimic addition and all except MAL2 de-repressed upon adding virus (Figures S5M–S5P). Our quantitative model outlines several factors controlling HCV-induced de-repression of host mRNA targets, namely, the expression level of the target mRNA, mRNA-miR-122 binding strength, and the number of sites on the target mRNA.

A miR-15-Dependent HCV Redirects miRNA Sequestration

To go beyond the correlative connection between our CLIP, RNA-seq, and modeling results, we set out to confirm the

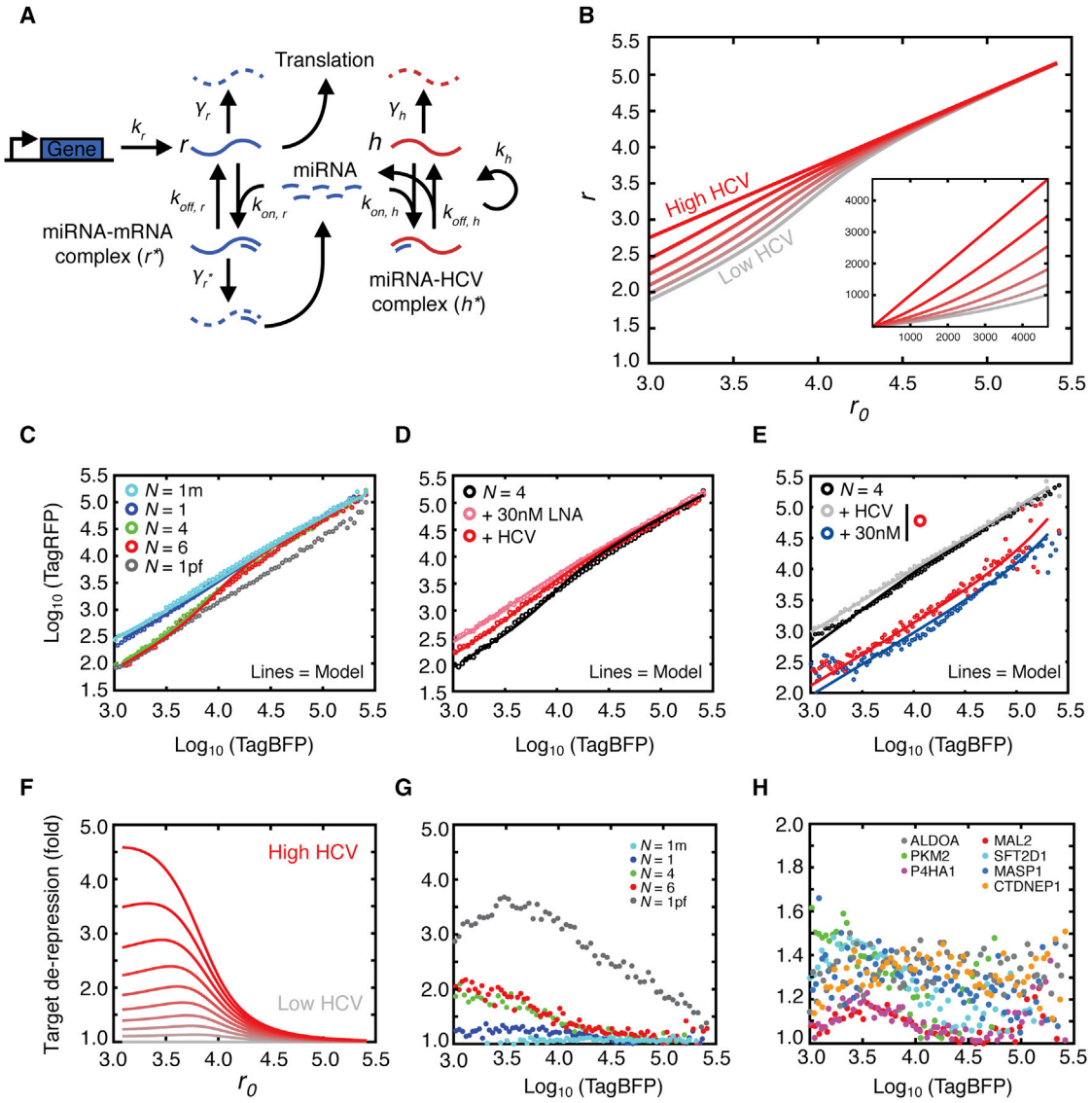

Figure 6. Quantitative Modeling of miR-122 Sequestration by HCV

(A) Illustration of model reactions for miR-122 dynamics, including transcription and translation of a target mRNA, binding to miR-122 and decay of mRNA species. HCV RNA can replicate, be degraded, or bind miR-122, and functionally sequestering miR-122 and leading to de-repression of mRNA targets.

(B) Increasing amounts of HCV or a relative increase in binding strength at miR-122 sites leads to changes in single-cell gene expression as compared to unregulated targets, with stronger effects at the low mRNA expression levels. Parameters used are fitted from data in (C). Each curve, from bottom to top represents a 20% reduction in the available miRNA pool by HCV. Inset displays model on a linear scale.

(C) Model fitting of the steady-state approximation to experimental data while increasing the number of binding sites corresponding to changes in total binding strength.

(D) Model fitting for the N = 4 case showing a 50% reduction in the miRNA pool by HCV modeled by a proportional change in the theta parameter.

(E) Model fitting for the N = 4 construct under 30 nM miR-122 mimic addition ± HCV infection.

(F) Increasing HCV:miR-122 binding strength or HCV RNA abundance in the model results in functional de-repression of miR-122 targets. Each curve, from bottom to top, represents a 10% decrease in the available miR-122 pool by HCV.

(G and H) Experimental HCV induced derepression of synthetic miR-122 binding site constructs (G) or endogenous 3′ UTRs with miR-122 binding sites (H). See also Figure S5 and S6.

sponge effect by swapping the miRNA tropism of the virus to determine if the miR-122 sponge could be redirected to the targets of another miRNA. We selected miR-15a/b, as these miRNAs had a sufficiently altered but GC-rich seed, and maintained the auxiliary pairing at nucleotides 2–3 and 30–31 of the viral genome (Machlin et al., 2011) (Figures 7A and S7A). In total, miR-15a/b constituted 5.3% ± 1.2% of miRNA identified via miRNA-CLIP, compared to 4.9% ± 2.0% for miR-122 (Table S1 and Figure S7A). An electroporated miR-15 variant HCV luciferase reporter virus (m15) was viable, and replicated to within

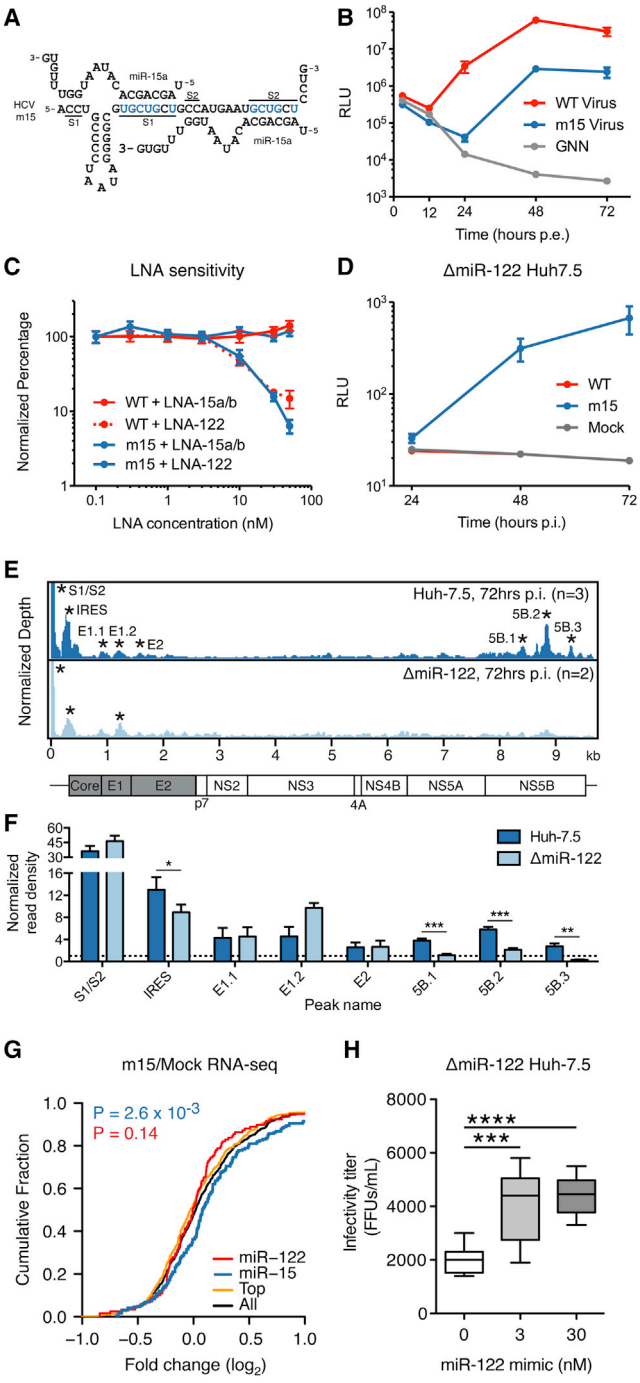

Figure 7. Exchanging HCV miRNA Tropism Redirects Functional miRNA Sequestration

(A) Base pairing diagram of miR-15a onto the mutated m15 HCV RNA. Base changes from the WT at S1 and S2 are highlighted in blue.

(B) Luciferase measurements of supernatants from WT and m15 HCV reporter virus electroporations (± SD). Non-replicating GNN control is shown.

(C) Dose response of WT and m15 reporter viruses following pre-treatment with LNA inhibitors of miR-122 or miR-15a/b at indicated concentrations, measured at 96 hr post-infection (±SD).

(D) Time course post-infection of ΔmiR-122 Huh-7.5 cells of indicated viruses (±SD).

one log of the WT virus after 72 hr (Figure 7B). Notably, the miR-15 virus was resistant to increasing concentrations of LNA122 (IC_{50} > 50 nM) but susceptible to LNA15a/b (IC_{50} = 10 nM) (Figure 7C). Similar results were obtained with non-reporter viruses through measuring HCV replication, spread of infection and virus titers (Figures S7B–S7G). Unlike WT virus, the m15 virus was viable in ΔmiR-122 cells (Figure 7D), thus demonstrating complete HCV replication independent of miR-122.

AGO binding on the m15 virus in Huh-7.5 cells largely mirrored results observed with WT virus (Figure 7E, top). Interestingly, we observed reduced AGO binding in ΔmiR-122 cells for the m15 virus in IRES and NS5B peaks harboring conserved miR-122 seeds, further suggesting miR-122 dependence for AGO binding in these regions (Figure 7E and 7F).

Turning our attention to the host, we measured the effect on the miR-15 targetome due to m15 virus replication via RNA-seq and confirmed de-repression specific to miR-15 targets while no longer observing effects on the miR-122 target network (Figure 7G). These results highlight the causal nature of an HCV-induced miRNA sponge as both functional and somewhat modular. We note that the m15 virus sponge effect was generally weaker than for the WT virus, likely due to the lower replication level observed and possibly to binding of the miR-15 family member, miR-16, which shares the seed site but may not be able to engage the m15 genome due to lack of auxiliary pairing (Figure S7A). Modification of the HCV 5′UTR could have direct effects on viral replication, and may explain the slight attenuation observed for the m15 virus (Figure 7B).

To further evaluate pro- or anti-viral effects of miR-122 abundance on the m15 virus, we measured m15 virus replication in ΔmiR-122 cells after re-introducing miR-122 at various concentrations. We observed a slight but significant increase in secreted m15 virus levels upon re-introducing miR-122 (Figure 7H). RNA levels and percent of infected cells were also increased in m15 infected ΔmiR-122 cells upon restoring miR-122 levels (Figures S7H and S7I). Conversely, we observed a significant reduction in viral titers after LNA-122 treatment of m15 infected Huh-7.5 cells (Figure S7G). Taken together, these results suggest that miR-122 sequestration by HCV replication confers a slightly less pro-viral cellular environment; an effect

(E) AGO binding map of m15 virus infection in WT Huh-7.5 (top) or ΔmiR-122 Huh-7.5 cells (bottom). Data were normalized to total cellular read depth for cross track comparison. Statistically significant peaks per track are named by location and are indicated by asterisks.

(F) AGO binding in significant peaks from (E) shown as normalized read densities calculated per dataset. Two-sided Student's t test used. Error bars, ± SD.

(G) CDF plot of the log_2 fold change in mRNA expression between HCV m15 infected and uninfected cells for all 3′UTR clusters containing indicated 7- to 8-mer seeds by family, from duplicate experiments at 96 hr post-infection. "Top" refers to the top 10 miRNA families, exclusive of miR-122 and miR-15. "All" refers to the top 50 miRNA families, inclusive of miR-122 and miR-15. Two-sided K-S test p value comparing miR-15 (blue) or miR-122 (red) clusters to "All" is shown.

(H) Infectivity titers of m15 virus in ΔmiR-122 Huh-7.5 complemented with exogenous miR-122 at indicated concentrations. One-way ANOVA with Bonferroni correction, whiskers, ± ranges.

Asterisks: ****p < 0.0001, ***p < 0.001, **p < 0.01, *p < 0.05. See also Figure S7.

that may be a small trade-off for the hugely beneficial role miR-122 plays directly in the viral life-cycle.

DISCUSSION

The aim of this study was to obtain an unbiased view of the miRNA interactome during HCV infection on both viral and cellular targets. We provide direct biochemical evidence of replication independent AGO association with HCV RNA at the 5′UTR in a number of infection contexts. Our results chiefly establish HCV RNA may act as a competitive inhibitor of miR-122 activity, an idea closely aligned with proposed roles for ceRNAs (Salmena et al., 2011). While both HCV RNA and ceRNAs share the theme of de-repressing a miRNA regulated network by increasing the pool of available targets through RNA expression, they differ in their mode of interaction with miRNAs. HCV genomic RNA critically requires miR-122 interaction to stabilize the viral genome and stimulate translation and replication, while most cellular miRNA targets are degraded upon encountering a miRNA. Moreover, unlike cellular mRNA targets, HCV genomic RNA is its own substrate for replication, and thus constitutes a positive feedback loop to sequester additional miR-122. These distinguishing features suggest different parameters for HCV versus ceRNA-based sponge effects on a miRNA target network. This is relevant in light of recent findings showing that endogenous miR-122 repression is only relieved when ceRNAs are forcibly expressed at super-physiological levels (Denzler et al., 2014). As HCV RNA represented at most between 1%–2% of CLIP reads following infection, our data suggest ceRNA activity may occur naturally at lower expression levels. Indeed, single-cell reporter measurements and mathematical modeling of the mRNA, HCV, and miRNA interplay suggest that HCV is able to de-repress host miR-122 targets, due to an approximate 2-fold reduction in available miR-122 under our experimental levels of HCV replication. Natural viral-derived miRNA sponges have been described previously (Cazalla et al., 2010; Lee et al., 2013) though no examples are currently known from RNA viruses. Whether this systems-level phenomenon occurs with other, more robust RNA virus infections remains to be explored.

The establishment of a miR-15-dependent HCV suggests that the miR-122 sponge effect is largely dispensable for the virus in the Huh-7.5 cell context. Indeed, we observed that LNA-122 slightly reduced m15 virus titers and that restoring miR-122 in ΔmiR-122 cells increased titers, suggesting that the miR-122 sponge may reflect a trade-off for the large, positive, and direct impact of miR-122 on WT HCV replication. Conceivably, HCV replication may exert enough pressure on miR-122 levels to de-repress targets such that the cellular environment is passively altered to negatively impact viral replication. Or more actively, there may exist miR-122 targets that act as sensors for low miR-122 levels, and by extension, the health of the hepatocyte. While future work will be needed to shed light on specific players involved in this process, our data suggest that viral replication faces a ceiling by reducing levels of an otherwise pro-viral miRNA.

How might the HCV miR-122 sponge impact a hepatocyte? Work with miR-122 knockout mice, which develop progressive liver disease that spontaneously results in HCC (Hsu et al., 2012; Tsai et al., 2012) suggests that miR-122 tumor suppressor activity is essential for long-term liver homeostasis. It is tantalizing to speculate that miR-122 sequestration in a chronic HCV infection may be a molecular link to the heterogeneous liver dysfunction that characterizes HCV-induced disease. Indeed, a number of miR-122 targets that we confirm or establish via CLIP and reporter measurements, such as P4HA1, PKM2, and MASP1 are known to be upregulated in fibrosis or HCC (Jung et al., 2011; Li et al., 2013a), with MASP1 notable for being specifically linked with HCV-associated HCC (Saeed et al., 2013). Still, there are challenges for a direct demonstration of an HCV miR-122 sponge in vivo. Our bulk cell measurements estimate 10-fold higher miR-122 levels in primary liver tissue versus hepatoma cell line derivatives (10^5 versus 10^4 estimate ranges per cell), while HCV levels per cell are estimated to range from 1 to 10^2 copies per hepatocyte (Kandathil et al., 2013), in contrast to Huh7 derivatives with 10^3 copies per cell. Yet, we observed functional HCV-induced de-repression in our single-cell reporter assay after addition of miR-122 in Huh-7.5 cells to mimic levels in vivo. Furthermore, we found specific de-repression of miR-122 targets in microarrays from HCV infected livers and from miravirsen-treated chimpanzees, supporting the existence of an HCV sponge effect in vivo. Unlike the >90% infection frequencies in Huh-7.5 cells, the percentage of infected hepatocytes in chronically infected patients based on in situ hybridization of liver biopsy tissue, ranges from as low as 0.07% to as high as 100%, with medians in the 20%–40% range (Liang et al., 2009; Pal et al., 2006). Combined with HCV genotype, dynamic replication variation within the liver, and host variability in innate immune responses (Sheahan et al., 2014), a complex picture of HCV infection emerges that would largely mask observations of HCV sponge effects in bulk cell or tissue AGO-CLIP measurements. As it remains possible that functional effects of such a sponge may impact highly infected cells, our data highlight the possibility of searching for transcriptome level changes to the miR-122 target network in response to HCV infection in individual cells. The extension of CLIP and RNA-seq in single-cell and primary contexts provides a compelling platform to address these and other long-term disease driven changes to a miRNA target network.

EXPERIMENTAL PROCEDURES

Culture of Cell Lines, Generation and Characterization of WT and m15 HCV

Cell lines were cultured and generated as described in Supplemental Information. pJ6/JFH1-Clone2, pJ6/JFH-Clone2-5AB-Ypet, and pJc1FLAG(p7-nsGluc2A) are fully infectious HCV non-reporter and reporter viruses, respectively, that have been previously described (Catanese et al., 2013; Horwitz et al., 2013; Marukian et al., 2008). To construct miR-15-dependent viruses in both backgrounds, we used an overlap PCR mutagenesis strategy. HCV cloning, RNA transcription, electroporation, infection, and related virus assays are described in detail in the Supplemental Information.

Argonaute HiTS-CLIP Analysis

Argonaute CLIP was performed generally following previous work (Chi et al., 2009), (Moore et al., 2014). Poly-G CLIP is a direct adaptation of the single linker ligation BrdU CLIP protocol (Weyn-Vanhentenryck et al., 2014). Relevant details pertaining to the CLIP protocol, multiplexed library preparation, and bioinformatic analysis are described in full in the Supplemental Information.

mRNA-Seq Library Construction

mRNA-seq libraries were prepared from Trizol extracted RNA following Illumina TruSeq protocols for poly-A selection, fragmentation, and adaptor ligation. Multiplexed libraries were sequenced as 100 nt single-end runs on either HiSeq-2000 or MiSeq platforms.

Luciferase Reporter Assays

Luciferase reporter vectors were cloned by inserting short oligonucleotides or PCR amplified target 3′UTRs into psiCHECK-2. The sequence of DNA oligonucleotides used for cloning are found in Table S7. Huh-7.5 cells were transfected over night with 2.56 nM final concentration LNA122 (Exiqon) or miR-122 mimic (Thermo Fisher) using RNAi/MAX (Invitrogen). Alternatively, cells were infected with HCV (J6/JFH1-clone2), MOI = 3 overnight. Twenty-four hours later, cells were transfected with 1 ng/well psiCHECK-2 reporter plasmid using Lipofectamine2000 (Invitrogen) and incubated over night before lysis in Passive Lysis Buffer and evaluation of luciferase levels using the Dual Luciferase Reporter Assay (Promega) on a Omega Fluorostar reader (BMG Labtech).

Single-Cell Reporter Measurements

Construction of miR-122 fluorescent reporters largely mirrored previous work with miR-20 (Mukherji et al., 2011). For a list of primers used in plasmid construction, please refer to Table S7. For flow cytometry, cells were run on a MACSQuant VYB flow cytometer (Miltenyi Biotec) after fixation to detect TagBFP, TagRFP, and Ypet signals. The raw FACS data were analyzed with FlowJo software to gate single, intact cells according to their forward (FSC-A) and side (SSC-A) scatter profiles. HCV-positive cells were gated on the basis of Ypet signal above uninfected background. Untransfected cells were used to characterize the cellular autoflourescence in BFP and RFP channels, from which we subtracted the mean plus two SD of the autofluorescent signal for each channel in transfected cells. Cells with BFP and RFP fluorescence levels less than 0 after background subtraction were excluded from further analyses. Data were log-transformed and binned according to BFP levels, and the mean RFP signal was calculated for each BFP bin.

ACCESSION NUMBERS

HiTS-CLIP and RNA-seq data have been deposited in the GEO under accession number GSE64680.

SUPPLEMENTAL INFORMATION

Supplemental Information includes Extended Experimental Procedures, seven figures, and seven tables and can be found with this article online at http://dx.doi.org/10.1016/j.cell.2015.02.025.

AUTHOR CONTRIBUTIONS

J.M.L. conceived the project; J.M.L., T.K.H.S., C.M.R., and R.B.D. designed the experiments; J.M.L., T.K.H.S, K.S.S., A.M., J.J.F., E.N., and M.T.C. performed the experiments; C.N.T. constructed Huh-7.5 TetON cells; Y.P.J and I.M.J provided clinical samples; J.M.L and T.D. developed the mathematical model; J.M.L, T.K.H.S, and T.D. analyzed the data; J.M.L, T.K.H.S, T.D., C.M.R., and R.B.D. wrote the manuscript with input from all authors.

ACKNOWLEDGMENTS

We thank C. Zhang for bioinformatics support; M. Moore for flow cytometry assistance; the Rockefeller Genomics Resource Center; and M.E. Castillo, S.M. Pecoraro Di Vittorio, J. Palarca, J. Sable, B. Hough-Loomis, and J. Smith for excellent technical and administrative assistance. Lastly, we thank members of the Darnell and Rice labs for invaluable advice. This study was supported by grants from the Public Health Service, NIH, NIAID (AI099284, AI072613, AI075099, AI091707, AI090055), NINDS (NS034389, NS081706), Office of the Director through the NIH Roadmap for Medical Research (DK085713), NCI (CA057973), The Rockefeller University Center for Clinical and Translational Science (UL1RR024143), the Center for Basic and Translational Research on Disorders of the Digestive System through the generosity of the Leona M. and Harry B. Helmsley Charitable Trust, the Greenberg Medical Research Institute, and the Starr Foundation. J.M.L. was supported by a David Rockefeller Graduate Student Fellowship. T.K.H.S. was supported by a Postdoctoral Fellowship and a Sapere Aude Research Talent Award from The Danish Council for Independent Research. C.N.T. was supported by an HHMI International Predoctoral Fellowship. M.T.C. was supported by the Rockefeller University Women and Science Fellowship. R.B.D. is an investigator of the Howard Hughes Medical Institute.

Received: August 2, 2014
Revised: November 26, 2014
Accepted: January 30, 2015
Published: March 12, 2015

REFERENCES

Bartel, D.P. (2009). MicroRNAs: target recognition and regulatory functions. Cell *136*, 215–233.

Castoldi, M., Vujic Spasic, M., Altamura, S., Elmén, J., Lindow, M., Kiss, J., Stolte, J., Sparla, R., D'Alessandro, L.A.L., Klingmüller, U., et al. (2011). The liver-specific microRNA miR-122 controls systemic iron homeostasis in mice. J. Clin. Invest. *121*, 1386–1396.

Catanese, M.T., Loureiro, J., Jones, C.T., Dorner, M., von Hahn, T., and Rice, C.M. (2013). Different requirements for scavenger receptor class B type I in hepatitis C virus cell-free versus cell-to-cell transmission. J. Virol. *87*, 8282–8293.

Cazalla, D., Yario, T., and Steitz, J.A. (2010). Down-regulation of a host microRNA by a Herpesvirus saimiri noncoding RNA. Science *328*, 1563–1566.

Chang, J., Nicolas, E., Marks, D., Sander, C., Lerro, A., Buendia, M.A., Xu, C., Mason, W.S., Moloshok, T., Bort, R., et al. (2004). miR-122, a mammalian liver-specific microRNA, is processed from hcr mRNA and may downregulate the high affinity cationic amino acid transporter CAT-1. RNA Biol. *1*, 106–113.

Chi, S.W., Zang, J.B., Mele, A., and Darnell, R.B. (2009). Argonaute HITS-CLIP decodes microRNA-mRNA interaction maps. Nature *460*, 479–486.

Darnell, J.C., Van Driesche, S.J., Zhang, C., Hung, K.Y.S., Mele, A., Fraser, C.E., Stone, E.F., Chen, C., Fak, J.J., Chi, S.W., et al. (2011). FMRP stalls ribosomal translocation on mRNAs linked to synaptic function and autism. Cell *146*, 247–261.

Denzler, R., Agarwal, V., Stefano, J., Bartel, D.P., and Stoffel, M. (2014). Assessing the ceRNA hypothesis with quantitative measurements of miRNA and target abundance. Mol. Cell *54*, 766–776.

Esau, C., Davis, S., Murray, S.F., Yu, X.X., Pandey, S.K., Pear, M., Watts, L., Booten, S.L., Graham, M., McKay, R., et al. (2006). miR-122 regulation of lipid metabolism revealed by in vivo antisense targeting. Cell Metab. *3*, 87–98.

Gatfield, D., Le Martelot, G., Vejnar, C.E., Gerlach, D., Schaad, O., Fleury-Olela, F., Ruskeepää, A.-L., Oresic, M., Esau, C.C., Zdobnov, E.M., and Schibler, U. (2009). Integration of microRNA miR-122 in hepatic circadian gene expression. Genes Dev. *23*, 1313–1326.

Haecker, I., Gay, L.A.L., Yang, Y., Hu, J., Morse, A.M.A., McIntyre, L.M.L., and Renne, R. (2012). Ago HITS-CLIP expands understanding of Kaposi's sarcoma-associated herpesvirus miRNA function in primary effusion lymphomas. PLoS Pathog. *8*, e1002884–e1002884.

Hafner, M., Landthaler, M., Burger, L., Khorshid, M., Hausser, J., Berninger, P., Rothballer, A., Ascano, M., Jr., Jungkamp, A.-C.A., Munschauer, M., et al. (2010). Transcriptome-wide identification of RNA-binding protein and microRNA target sites by PAR-CLIP. Cell *141*, 129–141.

Henke, J.I., Goergen, D., Zheng, J., Song, Y., Schüttler, C.G., Fehr, C., Jünemann, C., and Niepmann, M. (2008). microRNA-122 stimulates translation of hepatitis C virus RNA. EMBO J. *27*, 3300–3310.

Horwitz, J.A., Dorner, M., Friling, T., Donovan, B.M., Vogt, A., Loureiro, J., Oh, T., Rice, C.M., and Ploss, A. (2013). Expression of heterologous proteins

flanked by NS3-4A cleavage sites within the hepatitis C virus polyprotein. Virology *439*, 23–33.

Hsu, S.-H., Wang, B., Kota, J., Yu, J., Costinean, S., Kutay, H., Yu, L., Bai, S., La Perle, K., Chivukula, R.R., et al. (2012). Essential metabolic, anti-inflammatory, and anti-tumorigenic functions of miR-122 in liver. J. Clin. Invest. *122*, 2871–2883.

Janssen, H.L.A., Reesink, H.W., Lawitz, E.J., Zeuzem, S., Rodriguez-Torres, M., Patel, K., van der Meer, A.J., Patick, A.K., Chen, A., Zhou, Y., et al. (2013). Treatment of HCV infection by targeting microRNA. N. Engl. J. Med. *368*, 1685–1694.

Jopling, C.L., Yi, M., Lancaster, A.M., Lemon, S.M., and Sarnow, P. (2005). Modulation of hepatitis C virus RNA abundance by a liver-specific MicroRNA. Science *309*, 1577–1581.

Jopling, C.L., Schütz, S., and Sarnow, P. (2008). Position-dependent function for a tandem microRNA miR-122-binding site located in the hepatitis C virus RNA genome. Cell Host Microbe *4*, 77–85.

Jung, C.J.C., Iyengar, S., Blahnik, K.R.K., Ajuha, T.P.T., Jiang, J.X.J., Farnham, P.J.P., and Zern, M. (2011). Epigenetic modulation of miR-122 facilitates human embryonic stem cell self-renewal and hepatocellular carcinoma proliferation. PLoS ONE *6*, e27740–e27740.

Kandathil, A.J., Graw, F., Quinn, J., Hwang, H.S., Torbenson, M., Perelson, A.S., Ray, S.C., Thomas, D.L., Ribeiro, R.M., and Balagopal, A. (2013). Gastroenterology *145*, 1404–1413.e1410.

Lanford, R.E., Hildebrandt-Eriksen, E.S., Petri, A., Persson, R., Lindow, M., Munk, M.E., Kauppinen, S., and Ørum, H. (2010). Therapeutic silencing of microRNA-122 in primates with chronic hepatitis C virus infection. Science *327*, 198–201.

Lee, S., Song, J., Kim, S., Kim, J., Hong, Y., Kim, Y., Kim, D., Baek, D., and Ahn, K. (2013). Selective degradation of host MicroRNAs by an intergenic HCMV noncoding RNA accelerates virus production. Cell Host Microbe *13*, 678–690.

Lewis, B.P., Burge, C.B., and Bartel, D.P. (2005). Conserved seed pairing, often flanked by adenosines, indicates that thousands of human genes are microRNA targets. Cell *120*, 15–20.

Li, Y.-P., Gottwein, J.M., Scheel, T.K., Jensen, T.B., and Bukh, J. (2011). MicroRNA-122 antagonism against hepatitis C virus genotypes 1-6 and reduced efficacy by host RNA insertion or mutations in the HCV 5′ UTR. Proc. Natl. Acad. Sci. USA *108*, 4991–4996.

Li, J., Ghazwani, M., Zhang, Y., Lu, J., Li, J., Fan, J., Gandhi, C.R., and Li, S. (2013a). miR-122 regulates collagen production via targeting hepatic stellate cells and suppressing P4HA1 expression. J. Hepatol. *58*, 522–528.

Li, Y., Masaki, T., Yamane, D., McGivern, D.R., and Lemon, S.M. (2013b). Competing and noncompeting activities of miR-122 and the 5′ exonuclease Xrn1 in regulation of hepatitis C virus replication. Proc. Natl. Acad. Sci. USA *110*, 1881–1886.

Liang, Y., Shilagard, T., Xiao, S.Y., Snyder, N., Lau, D., Cicalese, L., Weiss, H., Vargas, G., and Lemon, S.M. (2009). Visualizing hepatitis C virus infections in human liver by two-photon microscopy. Gastroenterology *137*, 1448–1458.

Licatalosi, D.D., Yano, M., Fak, J.J., Mele, A., Grabinski, S.E., Zhang, C., and Darnell, R.B. (2012). Ptbp2 represses adult-specific splicing to regulate the generation of neuronal precursors in the embryonic brain. Genes Dev. *26*, 1626–1642.

Machlin, E.S., Sarnow, P., and Sagan, S.M. (2011). Masking the 5′ terminal nucleotides of the hepatitis C virus genome by an unconventional microRNA-target RNA complex. Proc. Natl. Acad. Sci. USA *108*, 3193–3198.

Marukian, S., Jones, C.T., Andrus, L., Evans, M.J., Ritola, K.D., Charles, E.D., Rice, C.M., and Dustin, L.B. (2008). Cell culture-produced hepatitis C virus does not infect peripheral blood mononuclear cells. Hepatology *48*, 1843–1850.

Mas, V.R., Maluf, D.G., Archer, K.J., Yanek, K., Kong, X., Kulik, L., Freise, C.E., Olthoff, K.M., Ghobrial, R.M., McIver, P., and Fisher, R. (2009). Genes involved in viral carcinogenesis and tumor initiation in hepatitis C virus-induced hepatocellular carcinoma. Mol. Med. *15*, 85–94.

Moore, M.J., Zhang, C., Gantman, E.C., Mele, A., Darnell, J.C., and Darnell, R.B. (2014). Mapping Argonaute and conventional RNA-binding protein interactions with RNA at single-nucleotide resolution using HITS-CLIP and CIMS analysis. Nat. Protoc. *9*, 263–293.

Mukherji, S., Ebert, M.S., Zheng, G.X.Y., Tsang, J.S., Sharp, P.A., and van Oudenaarden, A. (2011). MicroRNAs can generate thresholds in target gene expression. Nat. Genet. *43*, 854–859.

Nasheri, N., Singaravelu, R., Goodmurphy, M., Lyn, R.K., and Pezacki, J.P. (2011). Competing roles of microRNA-122 recognition elements in hepatitis C virus RNA. Virology *410*, 336–344.

Pal, S., Shuhart, M.C., Thomassen, L., Emerson, S.S., Su, T., Feuerborn, N., Kae, J., and Gretch, D.R. (2006). Intrahepatic hepatitis C virus replication correlates with chronic hepatitis C disease severity in vivo. J. Virol. *80*, 2280–2290.

Pang, P.S., Pham, E.A., Elazar, M., Patel, S.G., Eckart, M.R., and Glenn, J.S. (2012). Structural map of a microRNA-122: hepatitis C virus complex. J. Virol. *86*, 1250–1254.

Peng, X., Li, Y., Walters, K.-A., Rosenzweig, E.R., Lederer, S.L., Aicher, L.D., Proll, S., and Katze, M.G. (2009). Computational identification of hepatitis C virus associated microRNA-mRNA regulatory modules in human livers. BMC Genomics *10*, 373.

Riley, K.J., Rabinowitz, G.S., Yario, T.A., Luna, J.M., Darnell, R.B., and Steitz, J.A. (2012). EBV and human microRNAs co-target oncogenic and apoptotic viral and human genes during latency. EMBO J. *31*, 2207–2221.

Saeed, A., Baloch, K., Brown, R.J.P., Wallis, R., Chen, L., Dexter, L., McClure, C.P., Shakesheff, K., and Thomson, B.J. (2013). Mannan binding lectin-associated serine protease 1 is induced by hepatitis C virus infection and activates human hepatic stellate cells. Clin. Exp. Immunol. *174*, 265–273.

Salmena, L., Poliseno, L., Tay, Y., Kats, L., and Pandolfi, P.P. (2011). A ceRNA hypothesis: the Rosetta Stone of a hidden RNA language? Cell *146*, 353–358.

Sedano, C.D., and Sarnow, P. (2014). Hepatitis C virus subverts liver-specific miR-122 to protect the viral genome from exoribonuclease Xrn2. Cell Host Microbe *16*, 257–264.

Sheahan, T., Imanaka, N., Marukian, S., Dorner, M., Liu, P., Ploss, A., and Rice, C.M. (2014). Interferon lambda alleles predict innate antiviral immune responses and hepatitis C virus permissiveness. Cell Host Microbe *15*, 190–202.

Shimakami, T., Yamane, D., Jangra, R.K., Kempf, B.J., Spaniel, C., Barton, D.J., and Lemon, S.M. (2012). Stabilization of hepatitis C virus RNA by an Ago2-miR-122 complex. Proc. Natl. Acad. Sci. USA *109*, 941–946.

Singaravelu, R., Russell, R.S., Tyrrell, D.L., and Pezacki, J.P. (2014). Hepatitis C virus and microRNAs: miRed in a host of possibilities. Curr Opin Virol *7*, 1–10.

Skalsky, R.L.R., Corcoran, D.L.D., Gottwein, E., Frank, C.L.C., Kang, D., Hafner, M., Nusbaum, J.D.J., Feederle, R., Delecluse, H.-J.H., Luftig, M.A.M., et al. (2012). The viral and cellular microRNA targetome in lymphoblastoid cell lines. PLoS Pathog. *8*, e1002484–e1002484.

Tsai, W.-C., Hsu, S.-D., Hsu, C.-S., Lai, T.-C., Chen, S.-J., Shen, R., Huang, Y., Chen, H.-C., Lee, C.-H., Tsai, T.-F., et al. (2012). MicroRNA-122 plays a critical role in liver homeostasis and hepatocarcinogenesis. J. Clin. Invest. *122*, 2884–2897.

Weyn-Vanhentenryck, S.M., Mele, A., Yan, Q., Sun, S., Farny, N., Zhang, Z., Xue, C., Herre, M., Silver, P.A., Zhang, M.Q., et al. (2014). HITS-CLIP and integrative modeling define the Rbfox splicing-regulatory network linked to brain development and autism. Cell Rep. *6*, 1139–1152.

Yamane, D., McGivern, D.R., Masaki, T., and Lemon, S.M. (2013). Liver injury and disease pathogenesis in chronic hepatitis C. Curr. Top. Microbiol. Immunol. *369*, 263–288.

Zhang, C., and Darnell, R.B. (2011). Mapping in vivo protein-RNA interactions at single-nucleotide resolution from HITS-CLIP data. Nat. Biotechnol. *29*, 607–614.

Zhuang, F., Fuchs, R.T., Sun, Z., Zheng, Y., and Robb, G.B. (2012). Structural bias in T4 RNA ligase-mediated 3′-adapter ligation. Nucleic Acids Res. *40*, e54–e54.